Ultrafine, self-crimp, and electret nano-wool for low-resistance and high-efficiency protective filter media against $PM_{0.3}$
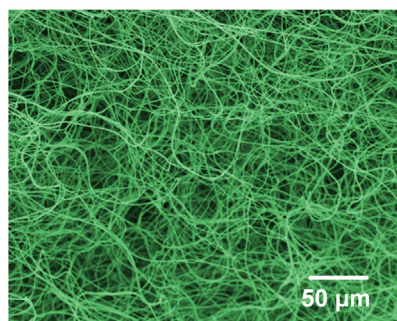
Yuyao Li [a], Leitao Cao [a], Xia Yin [a,b], Yang Si [a,b,*], Jianyong Yu [b], Bin Ding [b,*]

[a] State Key Laboratory for Modification of Chemical Fibers and Polymer Materials, College of Textiles, Donghua University, Shanghai 201620, China
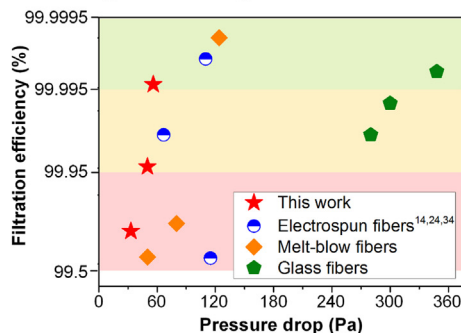[b] Innovation Center for Textile Science and Technology, Donghua University, Shanghai 200051, China

G R A P H I C A L   A B S T R A C T

A R T I C L E   I N F O

A B S T R A C T

Frequent outbreaks of emerging infectious diseases (EIDs) make personal protective filter media in high demand. Electrospun nanofibrous materials are proved to be very effective in resisting virus-containing fine particles owing to their small fiber diameters; however, hindered by the intrinsic close-packing character of fine fibers, electrospun filters suffer from a relatively high air resistance, thereby poor breathing comfort. Here, we report a biomimetic and one-step strategy to create ultrafine and curly wool-like nanofibers, named nano-wool, which exhibit fluffy assembly architecture and powerful electret effect. By achieving the online self-crimp and in-situ charging of nanofibers, the curly electret nano-wool shows a small diameter of ~0.6 µm (two orders of magnitude lower than natural wool: ~20 µm) and an ultrahigh porosity of 98.7% simultaneously, together with an ultrahigh surface potential of 13260 V (one order of magnitude higher than previous filters). The structural advantages and powerful electret effect enable nano-wool to show excellent filtration efficacy (>99.995% for $PM_{0.3}$) and low air resistance (55 Pa). Additionally, nano-wool can be easily scaled up, not only holding great industrial prospect in personal protective respirators, but also paving the way for developing next-generation wool in a cost-efficient and multifunctional form.

© 2020 Elsevier Inc. All rights reserved.

1. Introduction

The outbreaks of emerging infectious diseases (EIDs) can always trigger a public health emergency of international concern, taking a significant human toll and affect social stability. This issue is

highlighted by the outbreaks of Coronavirus Disease 2019 (COVID-19) recently. A report from the World Health Organization indicated that COVID-19 has spread to over 200 countries, territories or areas, causing over three million laboratory-confirmed cases and over 200 thousand deaths by 8 May 2020 [1–3]. Generally, viruses are transmitted through direct contact, droplets, and aerosols [4,5]. Among them, $PM_{2.5}$ and $PM_{0.3}$ (aerosol particles with diameters less than 2.5 and 0.3 μm, respectively) should be resisted especially owing to their ability to carry a mass of viruses and easily slip past our body's defences [6]. To protect the general public from being infected and control the transmission of EIDs, air filtration materials are highly demanded as the core of personal protective equipment. Unfortunately, the commonly used protective filter media are composed of melt-blown fibers, which are hard to achieve a high filtration efficiency of $PM_{2.5}$ under a low basis weight, let alone $PM_{0.3}$. This bottleneck is caused by the large micro-sized fiber diameters (>3 μm) and single filtration mechanism of size sieving [7,8]. The general strategy for increasing filtration efficiency is to increase the basis weight of filter media. The story is, however, this method would brings about the sharp increase of air resistance over materials, which means high breathing resistance for protective respirators [9]. Therefore, developing core materials that can provide effective protection and desirable breathing comfort simultaneously is long-sought-after yet largely unmet.

As the forefront of advanced materials, electrospun nanofibers (ESNs) have been proved to be capable of alleviating the conflict between filtration efficiency and pressure drop by virtue of their small fiber diameters (mostly <0.8 μm) [10,11]. More importantly, thanks to the applied high voltage, the resultant nanofibers are endowed with robust electret effect, which can improve the particle capture probability via electrostatic force, surprisingly, generating negligible effect on air flow [12,13]. Benefitting from the structural advantages and electret effect, ESNs with the same filtering capability as commercial products have been fabricated and their pressure drop can be generally controlled at ~100 Pa [14–16]. However, severely hindered by the inherent close-packing character of fine fibers, ESNs suffer from a bottleneck in improving porosity (generally <90%), seemingly unlikely to boost the filtration performance further [17,18]. Nature has been long considered as a source of inspiration in developing fascinating materials. From the biomimetic strategy, we notice that wool is more fluffy than the other natural fibers (such as cotton and fibrilia) when they have almost the same fiber diameters, which can be owed to the unique curly morphology. Unfortunately, wool is impossible to be applied to air filtration in view of its high cost and large fiber diameter (generally 20–30 μm, the finest wool is recorded to be >12 μm) [19]. Taking inspiration from curly wool, it can be expected that ESNs exhibiting curly morphology, combined with additional remarkable electret effect, can be an ideal filter medium; however, creating such materials is still highly challenging.

Herein, we present a biomimetic and one-step strategy to fabricate fluffy and electret filter media based on wool-like self-crimping nanofibers, named nano-wool, with powerful electrostatic effect, by simultaneously tailoring the trajectory and polarization of charged jets. The key to our design is that the self-crimp of nanofibers can be achieved online through control the exchanging rate between water and solvent molecules during jets flight; meanwhile, the electret property of nanofibers is dramatically enhanced by in situ boosting the dual-system (dipole and space) polarization charges. The resultant fluffy electret nano-wool felts (NWFs) exhibit integrated properties of high porosity, improved mechanical property and ultrahigh surface potential, making them an high-efficiency and low-resistance filter medium.

2. Experimental section

2.1. Fabrication of highly charged nano-wool

First, the precursor solutions used to obtained nano-wool were prepared by dissolving 16 wt% of polyvinylidene fluoride (PVDF, purity: 99.99%, M_w = 570,000, Solvey Co., Ltd., Belgium) in N,N-dimethylformamide (DMF, purity: 99.5%, Aladdin Chemistry Co., Ltd., China) containing 0.006 wt% lithium chloride (LiCl, purity: 99.9%, Aladdin Chemistry Co., Ltd., China). Then, the mixture was subjected to a continuous and vigorous stirring at room temperature for at least 8 h to obtain homogeneous solutions. Next, the as-prepared solutions were transferred into 5 syringes capped with metal nozzles (inner diameter: 0.7 mm), which were fixed at a sliding table with a moving speed of 30 cm min^{-1}. Once a high voltage of 25 kV was supplied to the nozzles, the solutions pumped out with a rate of 1 ml h^{-1} would easily form continuous jets, then being converted into nanofibers after a tip-to-collector distance of 20 cm. The solidified nanofibers were collected onto a metal roller (rotating speed of 30 rpm) wrapped with polyethylene non-wovens (filtration efficiency: 2%, pressure drop: 0 Pa). During the whole electrospinning process, the temperature was controlled at 25 ± 2 °C and the relative humidity was adjusted to 30 ± 3%,60 ± 3 %, and 90 ± 3%, resulting in PVDF-30, PVDF-60, and PVDF-90 nanofibers, respectively. Furthermore, highly charged wool-like nanofibers were also prepared according to the above-mentioned procedures with a fixed humidity of 90 ± 3% and by introducing 0.25, 0.5, and 0.1 wt% hydroxylapatite (HAP) nanoparticles (purity: 99.9%, Beijing DK Nano Technology Co., Ltd., China) introduced into the precursor solutions.

2.2. Characterization

The morphology and structure of nanofibers were observed by using scanning electron microscope (SEM, Vega 3, Tescan Ltd, Czech Republic). The fiber diameter distribution was estimated by the statistical analysis of 300 fibers randomly selected using an image analysis software (Adobe Photoshop CS6). The porosity (p) of the fabricated nanofibrous materials was obtained by: $p = (1 - m/\rho SH) \times 100\%$, where m, S, and H represent the base weight, area, and thickness of nanofibrous assemblies, and ρ is the density of PVDF. The detailed description and the structural parameters for the evaluation of porosity could be found in the Supplementary Methods and Table S1 (Supporting Information). The m and H were determined using a Mettler Toledo Micro balance (AT-20, readability of 2 μg) and a Labthink high-precision thickness gauge (CHYC2). The mechanical property of PVDF nanofibrous membranes and felts was tested via a XQ-1C tensile tester (Shanghai New Fiber Instrument Co., Ltd., China). The samples were cut into pieces with the size of 3 × 20 mm and fixed by the upper and lower collets. After setting the cross-head speed of 5 mm min^{-1}, the samples would be elongated until broke. During the elongation, computer would show the tensile stress–strain curves. 10 specimens from each membrane were tested for the evaluation of tensile behavior. The crystal phase structures of PVDF/HAP nano-wool was tested using Bruker XRD.

2.3. Evaluation of electret and air filtration performance

The electret property was evaluated using a non-contacting electrostatic instrument (VM54XQS, Quatek Inc., Shanghai, China). For each sample, 20 data was collected to calculate the average surface potential. And the evaluation for different samples was controlled with the same temperature (25 ± 2 °C) and humidity (45 ± 3%). The filtration performance including removing efficiency

toward particles with the most penetrated diameters (0.3 μm) and pressure drop was obtained via an automated filter tester (LZC-K, Huada Filter Technology Co., Ltd., China). The testing area was 100 cm^2 and three samples were selected for every kind of filter media. The detailed testing process has been depicted by our previous works and the information could also be found in Fig. S1 and Supplementary Methods (Supporting Information).

3. Results and discussion

3.1. Assembly model of fluffy nano-wool felts

We designed the high-performance air filtration materials mainly taking two criteria into account: (i) ESNs must possess high porosity to allow airflow to pass through easily; (ii) ESNs should be endowed with remarkable electret effect to ensure the effective capture of fine particles. The first requirement, also a bottleneck for nanofibrous materials, was overcame by creating curly PVDF nanofibers. To satisfy the second criterion, HAP nanoparticles, as an electrostatic enhancer, were introduced into PVDF solutions.

To achieve the online self-curling of ESNs, we propose a moisture-assisted electrospinning method to tailor the jet trajectory based on "nonsolvent induced phase separation" theory (Fig. 1a). Generally, charged jets experience bending perturbations driven by the Coulomb repulsion, then grow rapidly into a coil obeying the minimal kinetic energy principle [20]. To analyze the jet trajectory, a short segment of jet, composed of non-Newtonian fluid, can be modeled as many viscoelastic Maxwell elements in series (Fig. 1b). According to the Earnshaw's theorem, a specific unit B is not possible to maintain motionless only under the Coulomb forces of adjacent units (A and C), therefore easily moving toward the direction perpendicular to the line and reaching a new position B$_1$. The growth of the small bending perturbation can be characterized by the moving distance r, which is generally given by

$$r = r_0 \exp\left[\left(\frac{2e^2}{mL^3}\right)^{\frac{1}{2}} t\right] \tag{1}$$

where r$_0$ is the distance at t = 0, e stands for the charge, L represents the filament length, m is the mass, and t represents the time [21,22]. Obviously, there is a positive correlation betweenr and e. It should be mentioned that e is highly dependent on the contents of solvent within a jet infinitesimal because the solvent plays a role in accelerating ion movement. During the jet flying, solvent evaporation occurs all the time, leading to the formation of polymer-rich domains with low e and solvent-rich domains with high e (Fig. 1c) [23]. Attributing to the good compatibility between water and N,N-Dimethylformamide (DMF) in our system, high content of water molecules will promote the evaporation of solvent. Therefore, the jet paths can be tailored by controlling the exchanging rate between water molecules and DMF, then directly affecting the morphology of deposited nanofibers on collectors. Namely, jets at low RH (30%) experience a more vigorous bending perturbation than them at high RH (90%), and the degree of molecular entanglement within jets under 30% is lower than that under 90%, as illustrated by the different jet diameters in Fig. 1a. As a result, bead-on-string structured fibers would be inevitably yielded at RH of 30% owing to the partial molecular chains breaking, and curly fibers would be observed at RH of 90% due to the retraction of highly entangled molecular chains. As a proof of concept, we observed the SEM images of PVDF nanofibrous assemblies obtained from different RH (Fig. 1d–f). As expected, they exhibit totally different nanoarchitectures: bead-on-string structure at RH of 30%, smooth cylinder at RH of 60%, wool-like curly structure at RH of 90%, which was in accordance with the prediction. The

unique curly wool-like morphology was full covered, which could be proved by Fig. S2. In addition, the average fiber diameters obtained at 30%, 60%, and 90% RH were 307, 464, and 757 nm, respectively (Fig. S3a), further confirming the premature solidification of jets induced by moisture. The detailed diameter distribution could be found in Fig. S3b–d.

3.2. Fluffy architecture and performance evaluation

The precise tailoring of jet trajectory could not only render the formation of ultrathin nano-wool fibers, but also play a significant role in boosting the porosity of fibrous assemblies. Fig. 2a–c display the side views of PVDF nanofibrous assemblies obtained from RH of 30%, 60%, and 90% (PVDF-30, PVDF-60 and PVDF-90), all of which had the same basis weights. It can be intuitively observed that PVDF-30 NFMs showed a compact packing structure with beads embedded; some floating fibers appeared on PVDF-60 NFMs, implying that increasing RH contributed on increasing porosity. Notably, a highly fluffy structure with large pore volume was markedly highlighted when the fibrous assembly was fabricated under RH of 90%, beneficial for allowing airflow to pass through easily. Fig. S4 provided the in-situ deposition profile of PVDF nanofibers at the relative humidity of 90%, which could be another proof of fluffy architecture. The porosities of these three samples were calculated and presented in Fig. 2d. In accordance with the SEM images, the porosity increased from 70.7% to 80.4% with increasing RH from 30 to 60%, and further sharply rose to 98.7% at RH of 90%. To our best of knowledge, this ultrahigh porosity has never been achieved by an one-step electrospinning technology because the acknowledged advanced method, via reassembling fibers into a three-dimensional aerogel, to obtain high-porosity electrospun nanofibrous materials suffers from the tedious three-step pathway and high cost [24–26].

It can be easily understood that the self-crimp nanofibers makes for high porosity relying on their unique behavior of spatial support. However, given that PVDF is an acknowledged electret polymer, here we focused on a new perspective to elaborate the ultrahigh porosity of nano-wool felts – the electrostatic repulsion among fibers. The local electric field intensity (E) generated by an individual fiber could be deduced from the tested surface potentials (U). The surface potential was contributed by fibrous assemblies instead of individual fiber, which was obtained via a non-contacting method (inset of Fig. 2e). When the probe of the instrument moved above the samples with a height of h (h = 2 cm), the local surface potential was automatically shown in real time. The standard deviations of U were provided in the Table S2. The surface potential at (0, h) derived from samples with a certain radius of R can be expressed according to classical Gauss theorem:

$$U = \int_0^R \frac{dq}{4\pi\xi_0\sqrt{x^2 + h^2}}, \tag{2}$$

where dq is the charge carried by the micro ring with a width of dx, ξ_0 is the dielectric constant of PVDF, x is the location of the micro ring. Furthermore, dq is given by:

$$dq = \lambda dV = \lambda 2\pi x\phi dx \tag{3}$$

where λ is the charge density of individual fibers, which was the intrinsic property of electret fibers, dV is the volume of fibers within the micro ring, and ϕ is assumed to be the thickness [27,28].

It should be mentioned that this classical expression about dq didn't take the voids within samples into account. However, the as-prepared PVDF nanofibrous filter media are highly porous, therefore we propose a correction factor (τ) associated with the porosity (p), which could be defined as $\tau = (1 - p)$. In this case, dq could be revised as:
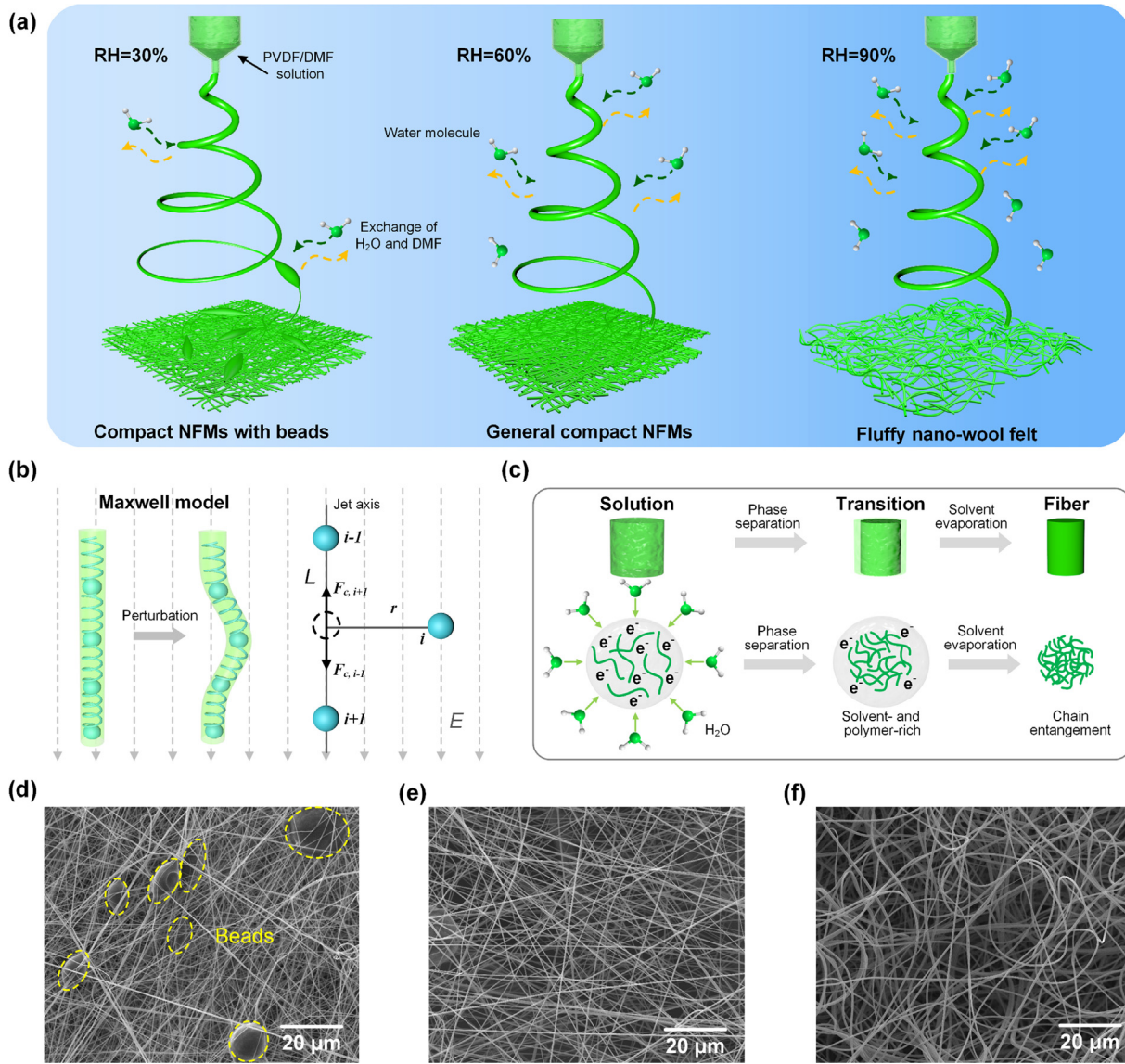
Fig. 1. Design principle and the resulting nano-wool materials. (a) Schematic diagrams describing the concept of the moisture-assisted online self-crimping of nanofibers. Three electrospinning conditions with designed relative humidity trigger the assembly of three different architectures: compact nanofibrous membranes (NFMs) with bead-on-string structure, general NFMs composed of straight nanofibers, and fluffy nano-wool. (b) Electrospun jet modeled by a system of viscoelastic Maxwell dumbbells and the jet perturbation driven by Earnshaw instability. (c) Illustration of the evolution from viscosity fluid to solid fibers. SEM images showing a proof of concept for the moisture-assisted strategy: (e) bead-on-string structured PVDF nanofibers from RH of 30%, (f) generally straight PVDF nanofibers from RH of 60%, and (g) wool-like curly PVDF nanofibers from RH of 90%.

$$dq = \lambda 2\pi x \phi \tau dx, \tag{4}$$

Combining the above-mentioned Eqs. (2), (3), and (4), revised U is easily obtained:

$$U = \int_0^R \frac{\lambda x \phi (1-p)}{2\xi_0 \sqrt{x^2 + h^2}} dx \tag{5}$$

Then, λ is deduced as following:

$$\lambda = \frac{2\xi_0 U}{\phi (1-p)\left(\sqrt{R^2 + h^2} - R\right)} \tag{6}$$

The charge density exhibited a rising trend with increasing the RH (Fig. S5). Furthermore, the electric field intensity (E) generated by individual fibers could be obtained according to the expression:

$$E = \frac{\lambda}{2\pi\xi_0 S} = \frac{U}{\pi\phi(1-p)\left(\sqrt{R^2 + h^2} - R\right)S} \tag{7}$$

Based on the tested surface potentials (U), combined with the already known structural (ϕ and p) and testing parameters (R and h), we could draw a conclusion that there were different dependencies between E and the distance from an individual fiber (S) for PVDF-30, PVDF-60, and PVDF-90 fibrous assemblies (Fig. 2e and Table S1). The dependent coefficients were 1.06×10^{12}, 1.63×10^{12}, and 3.96×10^{12} V m^{-2}. Fig. 2g presents an intuitive observation for the local electric field density by using a normalized color scale. Evidently, a narrow color range (from blue to cyan) was observed around PVDF-30 nanofibers with decreasing the distance, in strinking contrast to the situation of PVDF-60 and PVDF-90 nanofibers, which showed a relatively wider range (from blue to green and to red, respectively). In addition, the number of equipotential lines increased by 3 times from PVDF-30 to PVDF-90, also impling the enhancement of E. It should be mentioned that the dimensions plotted on Fig. 2f–h are meters because the deduction of all equations was based on the International System of Units.
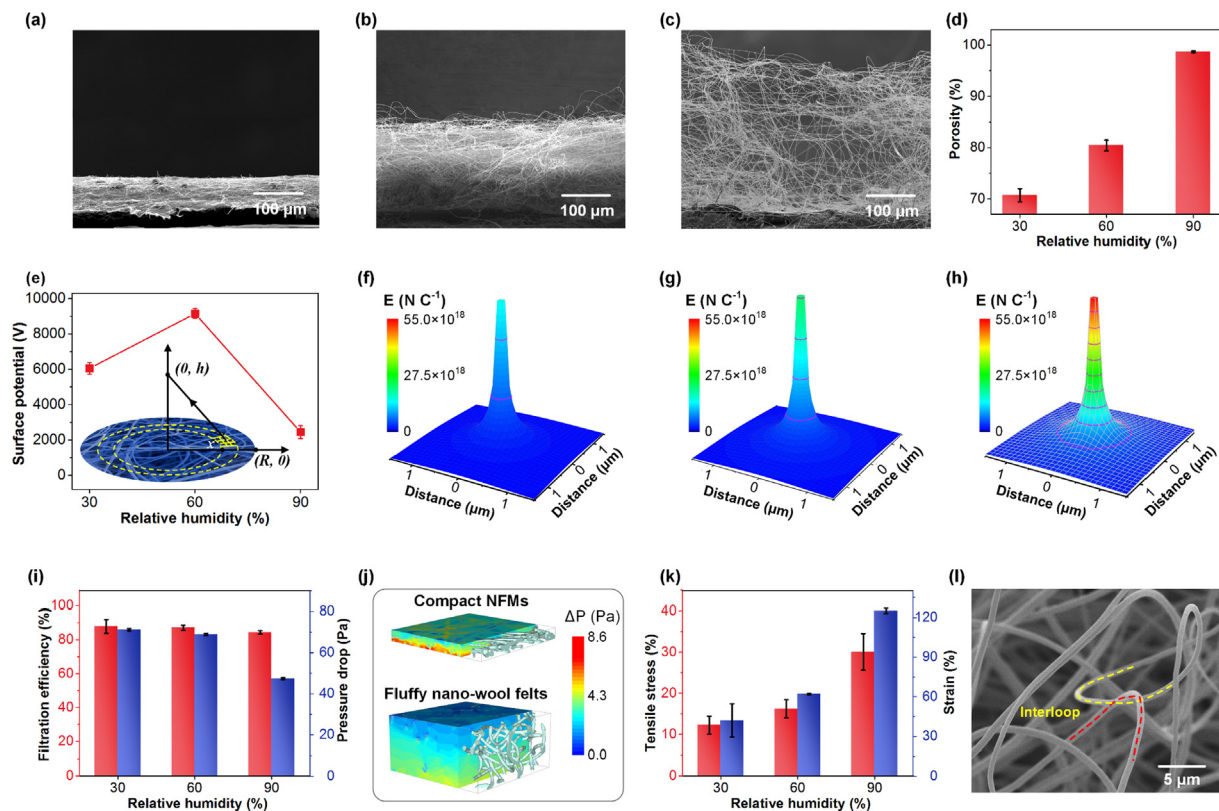
Fig. 2. Fluffy architecture and the improved filtration and mechanical properties. The side views of (a) PVDF-30 NFMs, (b) PVDF-60 NFMs and (c) PVDF-90 NWFs. (d) Porosity and (e) surface potential (error estimates from 20 tests) of PVDF nanofibrous materials obtained from different RH. Inset of (e) shows the testing schematic of surface potential. (f–h) The normalized electrostatic field intensity around individual fibers fabricated from humidities of (f) 30%, (g) 360, and (h) 90%, respectively. (i) Filtration performance of PVDF nanofibrous materials fabricated at different RH (error estimates from 3 tests). (j) 3D simulation showing the pressure field during airflow pass through PVDF-60 NFMs and PVDF-90 NWFs. (k) Tensile property of PVDF nanofibrous materials prepared from different RH (error estimates from 10 tests). (l) SEM image of PVDF-90 NWFs showing the interloop phenomenon between fibers.

These results confirmed that the highly fluffy architecture of NWFs was contributed by the electrostatic repulsion among fibers.

Encouraged by the unique curly morphology and the fluffy assembling structure of PVDF NWFs, we further investigated their filtration performance, as shown in Fig. 2i. The filtration efficiencies of three samples were almost the same, indicating their independence from humidity. This result was reasonable considering that the high charge density of individual nanofiber could be a compensation to the filtration efficiency that was sacrificed by large fiber diameters [29]. Surprisingly, the pressure drop was declined by over a third (from 71.2 to 47.4 Pa) by constructing NWFs, which was contributed by the rise of porosity. The airflow fields within compact NFMs and fluffy NWFs were simulated, as shown in Fig. 2j. The detailed simulation process could be found in the Supplementary Methods (Supporting Information). The airflow field utilizing color as scale demonstrated that NFMs presented colors ranging from cyan to red, in strikingly deviation to the dominant colors of blue and cyan for NWFs, suggesting the contribution of curl morphology on decreasing pressure drop. More surprisingly, Fig. 2k demonstrated that the tensile strength and elongation of PVDF-90 NWFs were 1.85 and 2 times of PVDF-60 NFMs, respectively. These results are in opposite to the common wisdom that a fluffy assembling structure tended to have an adverse effect on mechanical property. In other words, NFWs can be supposed to have overcome the bottleneck in obtaining a mechanically robust and fluffy fibrous materials. This discovery could be attributed to the interloop enhancing mechanism of curly nanofibers (Fig. 2l and Fig. S6a,b), which rendered a unique loop-stretching behavior (Fig. S6c) [30,31]. When subjected to the exter-

nal stress, NWFs firstly showed the morphology change from curly to straight, contributing high elongation. Additionally, the entanglement points between curly fibers triggered a double-fiber bearing phenomenon, which could be the reason for enhanced tensile strength. Based on the electrostatic force of PVDF wool-like nanofibers, nanofiber layer wouldn't detach from nonwovens under gravity. However, it has to be admitted that the nanofiber layer can be easily peeled off from nonwovens manually. To prevent the nanofibers from being detached from the substrate by shear forces during transport and processing, the needle-punching technology could be used to enhance the composite fastness owing to it generating less impact on fluffy architecture.

3.3. Nano-wool felts with enhanced electret effect

Endowing nanofibers with electrostatic electret effect has been identified as an attractive strategy to improve the filtration efficiency of filter media while not sacrificing their pressure drop. Encouraged by this point of view, hydroxylapatite (HAP) nanoparticles were introduced into the precursor solutions as a charge enhancer to in situ fabricate PVDF NWFs with remarkable electret effect. Fig. 3a–c display the representative SEM images of hybrid PVDF NWFs with HAP contents of 0.25, 0.5, and 1 wt%. Compared with the pure PVDF NWFs, the introduction of HAP with the content of less than 0.5 wt% seemed to have negligible impact on the homogeneity and coverage rate of curly morphology, which could be reflected by Fig. 3d and Fig. S7. In addition, the fiber diameter decreased from 757 to 578 nm with increasing HAP content from 0 to 0.5 wt% (Fig. 3d). However, further increasing the content
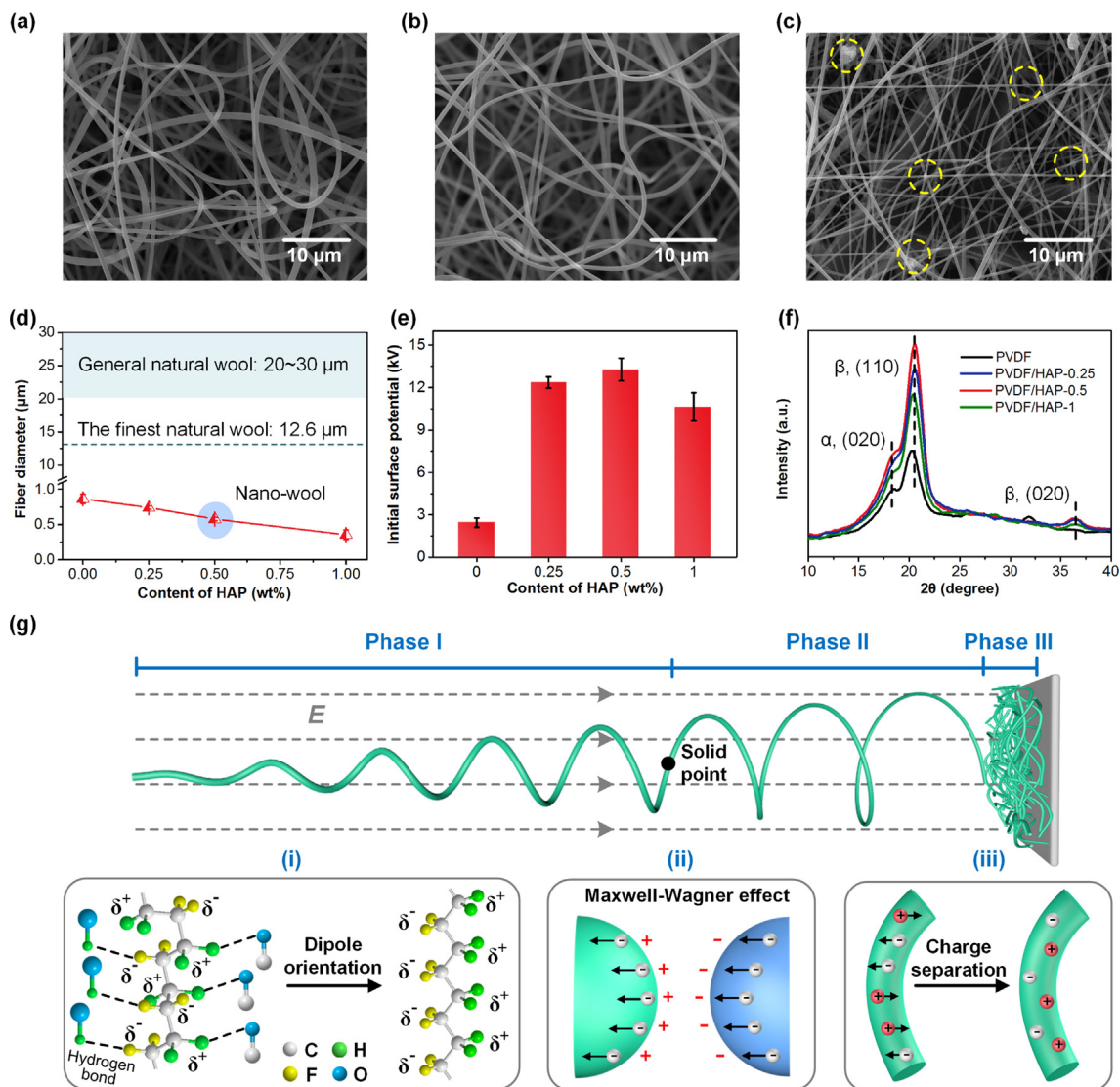
Fig. 3. NWFs with enhanced electret effect and the in-situ charging mechanism. SEM images of PVDF NWFs obtained from solutions containing HAP concentrations of (a) 0.25, (b) 0.5, and (c) 1 wt%. (d) Fiber diameter of PVDF/HAP NWFs and the comparison with natural wool (error estimates from 300 tests). (e) Surface potential (error estimates from 20 tests) and (f) XRD patterns of PVDF NWFs with various concentrations of HAP. (g) Schematic diagrams describing the proposed three-phase electret mechanism of electrospinning: (i) the dipolar orientation of PVDF and (ii) Maxwell-Wagner effect between PVDF and HAP during jets flying and the (iii) charge separation within solidified nanofibers.

of HAP to 1 wt% resulted in the disappearance of self-crimp nanofibers and the agglomeration of HAP. These phenomena appeared for the reason that HAP, as a typical kind of ionic crystal, could improve the conductivity of solutions and consequently endow composite PVDF/HAP jets with enlarged λ [32,33]. These results were essentially in accordance with the situation in low RH. Notably, the optimized PVDF/HAP-0.5 NWFs is two orders of magnitude lower in fiber diameter than natural wool, which exhibits the general diameter of 20–30 µm and the minimum diameter of 12.6 µm. Benefitting from the incorporation of HAP with proper content (0.5 wt%), the surface potential of PVDF/HAP NWFs achieved up to 13.26 kV (Fig. 3e), to the best of our knowledge, which is the highest value for electret ESNs yet [13,29]. The stability of electret property was investigated also. Fig. S8 indicated that PVDF nanowool with 0.5 wt% of HAP nanoparticles exhibited the highest surface potential after 120 min. The contribution of HAP to enhance the electret effect could be elaborated from three aspects. Firstly, HAP could trigger the crystal phase transition of PVDF from nonpolar α-phase to polar β-phase during jet flying, resulting in the

dipole charges, which was evidenced by Fig. 3f. The XRD spectra of PVDF NWFs with different HAP contents indicated that after incorporating HAP, the diffraction peak at $2\theta = 18.5°$, corresponding to the (0 2 0) plane reflection of α phase, was suppressed; meanwhile, the diffraction peak at $2\theta = 20.8°$, originating from the sum of (1 1 0) and (2 0 0) plane reflections of β phase, was enhanced. In addition, new peak at $2\theta = 36.5°$ that was derived from the (0 2 0) reflection plane of β phase appeared [34]. These results demonstrated the crucial role of HAP in promoting the formation of β phase for PVDF. The primary principle of this conversion lied in the hydrogen bond interaction between HAP and PVDF, leading to the aligned arrangement of hydrogen and fluorine atoms on both side of carbon chains during jets flying (Fig. 3g) [35]. Another electret mechanism during electrospinning was the Maxwell-Wagner effect existing at the interface of PVDF and HAP. Under the external electrostatic field, charges would be driven to move along the same direction within PVDF and HAP. The intrinsically different electronic transport capabilities between PVDF and HAP resulted in a charge barrier, which is hard to

overcome. As a result, charges tend to accumulate at the interfacial zones instead of being transferred from one to another, leading to the formation of interfacial charges [36,37]. It is worth noting that we propose that the classical Maxwell-Wagner effect can serve as an essential electret mechanism for ESNs, which might be identified as a progress since it has been employed to analyze the interfacial charges of buck bi-layer materials conventionally. The formation of dipole and interfacial charges were reasonably presumed to happen before and after fiber solidifying, respectively, because the former requires the easy movement of molecular chains and the latter needs the stable interface between PVDF and HAP. For the solidified and deposited nanofibers on collector, HAP played a role of defects in PVDF matrix, which would be helpful for the charge separation, thereby resulting in abundant volume charges [29,38]. Previous researches aiming to improve the electret property of electrospun filter media only focus on space charges (including interfacial and volume charges) by simply adding electret particles, ignoring the interaction between charge enhancer and polymer matrix. As such, this is the first report on achieving the synchronous improvement of dual-system (dipolar and space) electret charges via an efficient in-situ charging technology.

3.4. Nano-wool felts based high-performance air filters

We further investigated the filtration performance of various PVDF/HAP NWFs, the obtained results are presented in Fig. 4a.

With increasing the HAP contents from 0 to 0.5 wt%, the filtration efficiency of filter media was improved from 84.32 to 99.952%, which could be attributed to the elevation of surface potential. Meanwhile, a slight increase of pressure drop (from 47 to 50 Pa) was observed, implying that the introduction of 0.5 wt% HAP had almost no effect on the assembling structure of NWFs. It should be mentioned that the standard deviations for these results were too low to be observed, which was provided in the Table S3. This extremely low air resistance is less than 0.05% of the atmospheric pressure, which is negligible. The comprehensive filtration performance was generally evaluated by the quality factor (QF), which is given by: $QF = -\ln(1 - \eta)/\Delta P$, where η and ΔP represent the filtration efficiency and pressure drop, respectively [39]. Evidently, the optimal performance was achieved by PVDF/HAP-0.5 NWFs with the highest QF of 0.15 (Fig. S9). Further rising the content of HAP to 1 wt% gave rise to the deterioration of filtration performance, suggesting the adverse effect of excess nanoparticles. To give insight into the contribution of electret effect on filtration performance, we compared the capture behavior toward $PM_{0.3}$ and the airflow fields within both charged and neutral nanofibers (Fig. 4b). $PM_{0.3}$ was fed into the structural model for the reason that 0.3 μm is recognized as the most penetrating particle size. When the same amount of simulated aerosol particles were fed into the unit models, an unidirectional motion of particles was tracked within the neutral NWFs assembly. However, rebound trajectories of particles were observed within the charged NWFs
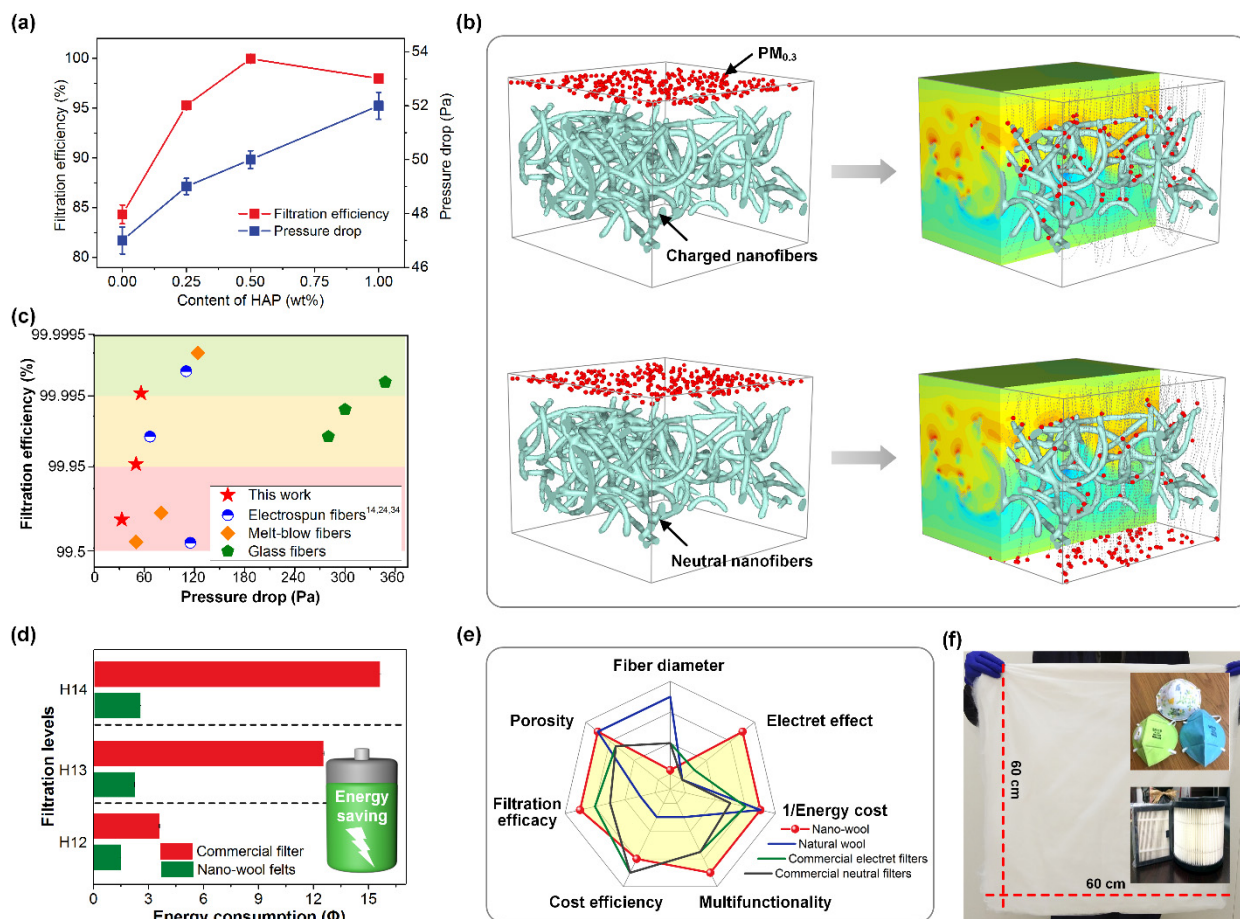
Fig. 4. Air filtration performance of NWFs and their application perspectives. (a) Filtration efficiency and pressure drop of PVDF NWFs as a function of HAP contents (error estimates from 3 tests). (b) Simulation illustrating the filtering process of charged and neutral nanofibers toward particles with the most penetrated size (0.3 μm). (c) Comparison of filtration performance among PVDF/HAP-0.5 NWFs, commercial mainstream filter media, and already reported ESN-based air filtration materials, showing that PVDF/HAP-0.5 NWFs are more energy-saving when they have the same filtration level. (d) Comparison of energy cost between commercial filters and NWFs. (e) A radar plot showing a comprehensive comparison among self-crimp nanofibers, natural wool, and commercial air filtration materials. (f) Large-scale production of NWFs and the resulting air filters.

model, suggesting that there was a re-capture phenomenon derived from the electrostatic force. Therefore, the capture ability was significantly enhanced by endowing the model with electret effect. In addition, the airflow fields before and after charging kept constant, which could be intuitively observed from the color distribution. In view of the multiplicity of practical applications, PVDF/HAP NWFs with different filtration levels including H12, H13 and H14 (with the filtration efficiency toward $PM_{0.3}$ of >99.5%, >99.95%, >99.995%) were further constructed by regulating the basis weight (Fig. 4c). As expected, PVDF/HAP NWFs exhibited lower pressure drops (33, 50, and 55 Pa) when they possessed the same filtration efficacy as commercial (glass fiber and melt-blown fibers) and three representative electrospun filter media (high-porosity aerogels, neutral and electret membranes) [14,24,34,40]. From a practical view of point, the energy consumption (Φ) of NWFs air filters was further estimated according to ASHRAE 1996, which specified the positive correlation between Φ and ΔP:

$$\Phi = \frac{v \Delta P t}{6356 \varpi_1 \varpi_2} \qquad (8)$$

where v is the feeding rate of polluted air, t stands for the operating time, ϖ_1 and ϖ_2 are the motor and fan efficiencies, which can be generally considered to be 0.9 and 0.75, respectively. Thus, given that the market air filtration materials are substituted by fluffy and electret NWFs, the energy cost could be significantly reduced by 59%, 82%, and 84% for air filters with filtration levels of H12, H13, and H14, respectively, highlighting the energy efficient advantage of NWFs air filters (Fig. 4d). Under the assumption of 1×10^7 air filtering units working in China, the decrease of 1 Pa could significantly save energy of 7.4×10^{10} kW h per year at the feeding rate of 1 m s^{-1}, thus, NWFs air filters are expected to save almost $6.3 billion in energy cost.

The advantages of NWFs over both natural wool and the available commercial filter media were highlighted, as qualitatively illustrated by Fig. 4e. From a structural point of view, NWFs overcame the bottleneck of nanofibers assembling densely by inheriting the unique curly morphology of natural wool and relying on the additional powerful electret effect. By virtue of the structure merits and superior electrostatic force, NWFs can achieve an optimal equilibrium relationship between the two conflict filtration factors, namely filtration efficiency and pressure drop. That is, compared with the existing commercial filter media, NWFs is more energy-saving when then have the same filtration efficacy. Natural wool, with an extremely fluffy architecture, might show small pressure drop; however, they has never been used as filter media, which is certainly associated with their coarse-fiber. In terms of the cost efficiency, ESN-based materials can be easily scaled up by using multi-needles. As shown in Fig. 4f, NWFs with a large size of 60×60 cm^2 could be fabricated and serve as the core materials of 20 masks or 3 filter elements. However, obtaining a natural wool assembly with the same area has to experience tedious procedures, such as raising sheep, shearing, removing impurities, spinning, weaving, and so on, which leading to the high cost of natural wool fabric. In contrast, PVDF has already been considered as a cost-effective industrial raw material. Representative companies like Solvey (Belgium) and Arkema (France) have been selling PVDF polymer for many years with the price of only ~30 dollars per kilogram. In addition, considering that polymers containing long perfluorooctyl ($-C_8F_{17}$) segments exhibit high bioaccumulation, environmental persistence and long-distance migration, PVDF is an environment-friendly polymer owing to the short perfluorooctyl segments ($-CH_2-CF_2-$) [41–43]. It has to be admitted that the production rate of NWFs is still lower than the commercial filter media that are fabricated from mature technologies including wet spinning and melt-blown. Finally, with regard to the multi-

functionality, the output voltages of various NFWs were measured considering that PVDF is featured with relatively high piezoelectric property (Fig. S10). PVDF/HAP-0.5 NFWs achieved the highest output voltage of ~4 V, superior to most of previous PVDF NFMs, suggesting that highly charged NWFs hold great potential to be the candidate of piezoelectric devices [44–46]. Moreover, based on that decreasing the fiber diameter has been acknowledged as one of the most effective way to improve the clothing comfort, the as-prepared NWFs are of great significance for developing highly comfortable garment with smart functions by virtue of their small fiber diameter and electret property [47].

4. Conclusions

In summary, we demonstrated a biomimetic and cost-effective strategy to controllably prepare highly fluffy and electret polyvinylidene fluoride (PVDF) nano-wool felts (NWFs) by employing a moisture-assisted self-crimping technology and in situ introducing hydroxylapatite (HAP) nanoparticles as charge enhancer. Through accelerate the exchanging rate between water and solvent molecules, the PVDF jet trajectories were precisely tailored and solidified into wool-like curly nanofibers showing a small diameter of ~0.6 μm and a ultrahigh porosity of 98.7%. Compared to the electrospun nanofiber-based aerogels featured with high porosity, PVDF NWFs showed advantages in terms of one-step fabrication [24–26]. Furthermore, benefitting from the hydrogen interaction and interfacial Maxwell-Wagner effect between PVDF and HAP, dual-system (dipole and space) electret charges were simultaneously boosted. The resulting PVDF/HAP NWFs showed absolutely advantages over traditional natural wool in dramatically declined fiber diameter and additional electrostatic effect. The ultrahigh surface potential of 13,260 V was significantly higher than the previously reported electrospun electret nanofibrous filter media [13,29,48]. The future work could focus on two aspects: the marketization of PVDF NWFs as high-efficiency and low-resistance filters, and the development of natural wool in a smart and multifunctional way.

CRediT authorship contribution statement

Yuyao Li: Conceptualization, Data curation, Writing - original draft. **Leitao Cao:** Software, Formal analysis. **Xia Yin:** Investigation. **Yang Si:** Methodology, Project administration. **Jianyong Yu:** Writing - review & editing. **Bin Ding:** Supervision, Validation, Funding acquisition.

Declaration of Competing Interest

The authors declare that they have no known competing financial interests or personal relationships that could have appeared to influence the work reported in this paper.

Acknowledgments

Appendix A. Supplementary data

Supplementary data to this article can be found online at https://doi.org/10.1016/j.jcis.2020.05.123.

References

[1] M. Bermejo, J.D. Rodriguez-Teijeiro, G. Illera, A. Barroso, C. Vila, P.D. Walsh, Ebola Outbreak Killed 5000 Gorillas, Science 314 (2006) 1564.

[2] M.I. Nelson, C. Viboud, A.L. Vincent, M.R. Culhane, S.E. Detmer, D.E. Wentworth, A. Rambaut, M.A. Suchard, E.C. Holmes, P. Lemey, Global migration of influenza a viruses in swine, Nat. Commun. 6 (2015) 6696.

[3] https://www.who.int/emergencies/diseases/novel-coronavirus-2019/situation-reports/

[4] M. Richard, R.A. Fouchier, Influenza a virus transmission via respiratory aerosols or droplets as it relates to pandemic potential, FEMS Microbiol. Rev. 40 (2016) 68.

[5] R. Tellier, Review of aerosol transmission of influenza a virus, Emerg. Infect. Dis. 12 (2006) 1657.

[6] T.H. Kao, S.K. Su, C.I. Su, A.W. Lee, J.K. Chen, Polyacrylonitrile microscaffolds assembled from mesh structures of aligned electrospun nanofibers as high-efficiency particulate air filters, Aerosol Sci. Tech. 50 (2016) 615.

[7] S. Jung, J. An, H. Na, J. Kim, Surface energy of filtration media influencing the filtration performance against solid particles, oily aerosol, and bacterial aerosol, Polymers 11 (2019) 1702139.

[8] A. Penconek, A. Jackiewicz, A. Moskal, Penetration of diesel exhaust particles (Deps) through fibrous filters produced using melt-blown technology, KONA Powder Part. J. (2015) 2015008.

[9] Q. Zhang, J. Welch, H. Park, C.Y. Wu, W. Sigmund, J.C.M. Marijnissen, Improvement in nanofiber filtration by multiple thin layers of nanofiber mats, J. Aerosol Sci. 41 (2010) 230.

[10] S. Sundarrajan, K.L. Tan, S.H. Lim, S. Ramakrishna, Electrospun nanofibers for air filtration applications, Procedia Eng. 75 (2014) 159.

[11] Y. Shen, D. Li, B. Deng, Q. Liu, H. Liu, T. Wu, Robust polyimide nano/microfibre aerogels welded by solvent-vapour for environmental applications, R. Soc. Open Sci. 6 (2019) 190596.

[12] K.S. Han, S. Lee, M. Kim, P. Park, M.H. Lee, J. Nah, Electrically activated ultrathin PVDF-TrFE air filter for high-efficiency $PM_{1.0}$ filtration, Adv. Funct. Mater. 29 (2019) 1903633.

[13] B.Y. Yeom, E. Shim, B. Pourdeyhimi, Boehmite nanoparticles incorporated electrospun nylon-6 nanofiber web for new electret filter media, Macromol. Res. 18 (2010) 884.

[14] H. Liu, S. Zhang, L. Liu, J. Yu, B. Ding, A fluffy dual-network structured nanofiber/net filter enables high-efficiency air filtration, Adv. Funct. Mater. 29 (2019) 1904108.

[15] D. Lv, R. Wang, G. Tang, Z. Mou, J. Lei, J. Han, C.D.S. Smedt, R. Xiong, C. Huang, Eco-friendly electrospun membranes loaded with visiblelight response nano-particles for multifunctional usages: high-efficient air filtration, dye scavenger and bactericide, ACS Appl. Mater. Interfaces 11 (2019) 12880–12889.

[16] H. Wang, S. Lin, S. Yang, X. Yang, J. Song, D. Wang, H. Wang, Z. Liu, B. Li, M. Fang, et al., High-temperature particulate matter filtration with resilient Yttria-stabilized ZrO_2 nanofiber sponge, Small 14 (2018) 1800258.

[17] Y. Si, Q. Fu, X. Wang, J. Zhu, J. Yu, G. Sun, B. Ding, Superelastic and superhydrophobic nanofiber-assembled cellular aerogels for effective separation of oil/water emulsions, ACS Nano 9 (2015) 3791–3799.

[18] Y. Si, J. Yu, X. Tang, J. Ge, B. Ding, Ultralight nanofibre-assembled cellular aerogels with superelasticity and multifunctionality, Nat. Commun. 5 (2014) 5802.

[19] https://bellatory.com/clothing/The-Rarest-Fabric-in-the-World

[20] H.D. Reneker, L.A. Yarin, H. Fong, S. Koombhongse, Bending instability of electrically charged liquid jets of polymer solutions in electrospinning, J. Appl. Phys. 87 (2000) 4531–4547.

[21] H.D. Reneker, L.A. Yarin, Electrospinning jets and polymer nanofibers, Polymer 49 (2008) 2387–2425.

[22] L.A. Yarin, S. Koombhongse, H.D. Reneker, Bending instability in electrospinning of nanofibers, J. Appl. Phys. 89 (2001) 3018.

[23] L.S. Shenoy, D.W. Bates, L.H. Frisch, E.G. Wnek, Role of chain entanglements on fiber formation during electrospinning of polymer solutions: Good solvent. Non-Specific Polymer-Polymer Interaction Limit, Polymer 46 (2005) 3372–3384.

[24] F. Deuber, S. Mousavi, L. Federer, M. Hofer, C. Adlhart, Exploration of ultralight nanofiber aerogels as particle filters: Capacity and efficiency, ACS Appl. Mater. Interfaces 10 (2018) 9069–9076.

[25] Z. Qian, Z. Wang, Y. Chen, S. Tong, M. Ge, N. Zhao, J. Xu, Superelastic and ultralight polyimide aerogels as thermal insulators and particulate air filters, J. Mater. Chem. A 6 (2018) 828.

[26] J. Nemoto, T. Saito, A. Isogai, Simple freeze-drying procedure for producing nanocellulose aerogel-containing, high-performance air filters, ACS Appl. Mater. Interfaces 7 (2015) 19809–19815.

[27] L. Nanis, W. Kesselman, Engineering applications of current and potential distributions in disk electrode systems, J. Electrochem. Soc. 118 (1971) 454–461.

[28] P. Wolfe, Eigenfunctions of the integral equation for the potential of the charged disk, J. Math. Phys. 12 (7) (1971) 1215–1218.

[29] S. Wang, X. Zhao, X. Yin, J. Yu, B. Ding, Electret polyvinylidene fluoride nanofibers hybridized by polytetrafluoroethylene nanoparticles for high-efficiency air filtration, ACS Appl. Mater. Interfaces 8 (2016) 23985–23994.

[30] D.L. Tijing, W. Choi, Z. Jiang, A. Amarjargal, C.-H. Park, R.H. Pant, I.-T. Im, S.C. Kim, Two-nozzle electrospinning of (MWNT/PU)/PU nanofibrous composite mat with improved mechanical and thermal properties, Curr. Appl. Phys. 13 (2013) 1247–1255.

[31] G. Dusserre, L. Balea, G. Bernhart, Elastic properties prediction of a knitted composite with inlaid yarns subjected to stretching: A coupled semi-analytical model, Compos. Part A-Appl. S. 64 (2014) 185–193.

[32] X. Zhao, S. Wang, X. Yin, Yu. Ji, B. Ding, Slip-effect functional air filter for efficient purification of $PM_{2.5}$, Sci. Rep. 6 (2016) 35472.

[33] X. Gao, Z.K. Li, J. Xue, Y. Qian, L.Z. Zhang, J. Caro, H. Wang, Titanium carbide Ti_3C_2Tx (Mxene) enhanced PAN nanofiber membrane for air purification, J. Membrane Sci. 586 (2019) 162–169.

[34] X. Li, C. Wang, X. Huang, T. Zhang, X. Wang, M. Min, L. Wang, H. Huang, S.B. Hsiao, Anionic surfactant-triggered steiner geometrical poly(vinylidene fluoride) nanofiber/nanonet air filter for efficient particulate matter removal, ACS Appl. Mater. Interfaces 10 (2018) 42891–42904.

[35] T. Huang, S. Yang, P. He, J. Sun, S. Zhang, D. Li, Y. Meng, J. Zhou, H. Tang, J. Liang, et al., Phase-separation-induced PVDF/graphene coating on fabrics toward flexible piezoelectric sensors, ACS Appl. Mater. Interfaces 10 (2018) 30732–30740.

[36] L.A. Shcherbachenko, V.S. Borisov, N.T. Maksimova, E.S. Baryshnikov, V.A. Karnakov, S.D. Marchuk, Ya.V. Ezhova, L.I. Ruzhnikov, Electret effect and electrotransport in disperse organic and inorganic systems, Tech. Phys. 54 (2009) 1372–1379.

[37] W.C. Ko, C.K. Tseng, W.J. Wu, C.K. Lee, Charge storage and mechanical properties of porous PTFE and composite PTFE/COC electrets, e-Polymers 10 (2010) 032.

[38] L.S. McCarty, M.W. George, Electrostatic charging due to separation of ions at interfaces: Contact electrification of ionic electrets, Angew. Chem. Int. Edit. 47 (2008) 2188–2207.

[39] C. Liu, P.-C. Hsu, H.-W. Lee, M. Ye, G. Zheng, N. Liu, W. Li, Y. Cui, Transparent air filter for high-efficiency $PM_{2.5}$ capture, Nat. Commun. 6 (2015) 6205.

[40] British Standard, High Efficiency Air Filters, EPA, HEPA and ULPA, 2009.

[41] J. Zhao, W. Zhu, X. Wang, L. Liu, J. Yu, B. Ding, Fluorine-free waterborne coating for environmentally friendly, robustly water-resistant, and highly breathable fibrous textiles, ACS Nano 14 (2020) 1045.

[42] M. Stucki, C. Kellenberger, M. Loepfe, W. Stark, Internal polymer pore functionalization through coated particle templating affords fluorine-free green functional textiles, J. Mater. Chem. A 4 (2016) 15197.

[43] M. Krafft, J. Riess, Selected physicochemical aspects of poly- and perfluoroalkylated substances relevant to performance, environment and sustainability – Part one, Chemosphere 129 (2015) 4.

[44] H. Parangusan, D. Ponnamma, M.A.A. AlMaadeed, Investigation on the effect of γ-irradiation on the dielectricand piezoelectric properties of stretchable PVDF/Fe–ZnO nanocomposites for self-powering devices, Soft Matter 14 (2018) 8803–8813.

[45] X. Chen, X. Han, Q.D. Shen, PVDF-based ferroelectric polymers in modern flexible electronics, Adv. Electron. Mater. 3 (2017) 1600460.

[46] M.M. Alam, S.K. Ghosh, A. Sultana, D. Mandal, An effective wind energy harvester by paper-ash mediated rapid synthesized ZnO nano-particle interfaced electrospun PVDF Fiber, ACS Sustain. Chem. Eng. 6 (2017) 292–299.

[47] B.A. McGregor, M. Naebe, Effect of fibre yarn and knitted fabric attributes associated with wool comfort properties, J. Text. I. 104 (2013) 606–617.

[48] X. Ding, Y. Li, Y. Si, X. Yin, J. Yu, B. Ding, Electrospun polyvinylidene fluoride/SiO_2 nanofibrous membranes with enhanced electret property for efficient air filtration, Compos. Commun. 13 (2019) 57–62.